



Article

Scavenging of Superoxide in Aprotic Solvents of Four Isoflavones That Mimic Superoxide Dismutase

Sandra Yu , Francesco Caruso, Stuart Belli and Miriam Rossi *

Department of Chemistry, Vassar College, Poughkeepsie, NY 12604, USA

* Correspondence: rossi@vassar.edu

Abstract: Isoflavones are plant-derived natural products commonly found in legumes that show a large spectrum of biomedical activities. A common antidiabetic remedy in traditional Chinese medicine, *Astragalus trimestris* L. contains the isoflavone formononetin (FMNT). Literature reports show that FMNT can increase insulin sensitivity and potentially target the peroxisome proliferator-activated receptor gamma, PPAR γ , as a partial agonist. PPAR γ is highly relevant for diabetes control and plays a major role in Type 2 diabetes mellitus development. In this study, we evaluate the biological role of FMNT, and three related isoflavones, genistein, daidzein and biochanin A, using several computational and experimental procedures. Our results reveal the FMNT X-ray crystal structure has strong intermolecular hydrogen bonding and stacking interactions which are useful for antioxidant action. Cyclovoltammetry rotating ring disk electrode (RRDE) measurements show that all four isoflavones behave in a similar manner when scavenging the superoxide radical. DFT calculations conclude that antioxidant activity is based on the familiar superoxide σ -scavenging mode involving hydrogen capture of ring-A H7(hydroxyl) as well as the π - π (polyphenol-superoxide) scavenging activity. These results suggest the possibility of their mimicking superoxide dismutase (SOD) action and help explain the ability of natural polyphenols to assist in lowering superoxide concentrations. The SOD metalloenzymes all dismutate $O_2^{\bullet-}$ to H_2O_2 plus O_2 through metal ion redox chemistry whereas these polyphenolic compounds do so through suitable hydrogen bonding and stacking intermolecular interactions. Additionally, docking calculations suggest FMNT can be a partial agonist of the PPAR γ domain. Overall, our work confirms the efficacy in combining multidisciplinary approaches to provide insight into the mechanism of action of small molecule polyphenol antioxidants. Our findings promote the further exploration of other natural products, including those known to be effective in traditional Chinese medicine for potential drug design in diabetes research.

Keywords: superoxide; free radicals; superoxide dismutase; diabetes; cyclovoltammetry; formononetin; isoflavones



Citation: Yu, S.; Caruso, F.; Belli, S.; Rossi, M. Scavenging of Superoxide in Aprotic Solvents of Four Isoflavones That Mimic Superoxide Dismutase. *Int. J. Mol. Sci.* **2023**, *24*, 3815. <https://doi.org/10.3390/ijms24043815>

Academic Editor: Albert Poater

Received: 1 January 2023

Revised: 28 January 2023

Accepted: 7 February 2023

Published: 14 February 2023



Copyright: © 2023 by the authors. Licensee MDPI, Basel, Switzerland. This article is an open access article distributed under the terms and conditions of the Creative Commons Attribution (CC BY) license (<https://creativecommons.org/licenses/by/4.0/>).

1. Introduction

Isoflavones, including formononetin (FMNT, 7-hydroxy-3-(4-methoxyphenyl)chromen-4-one), are bioactive phytochemicals that are abundant in legumes such as chickpeas, soy, beans and red clover [1]. These compounds are of nutritional and medicinal interest and are known as phytoestrogens because they bind with the β -estrogen receptor, a member of the nuclear hormone receptor (NHR) superfamily [2]. Additionally, FMNT is reported to have multiple biological activities, including neuroprotective, antitumor, antioxidant and anti-inflammatory effects in various in vitro and animal models [3–5]. Since literature reports show FMNT has moderate bioavailability, it is interesting to study for in vivo trials [6].

FMNT is also found in *Astragalus trimestris* L. (*Astragalus membranaceus* Moench) (*Fabaceae*), a common antidiabetic herbal remedy in traditional Chinese medicine [7]. Diabetes Mellitus is a serious global health issue, reaching a global prevalence of 10.5% across all adults aged 20–79 [8]. Insulin sensitivity is also promoted by the peroxisome proliferator-activated

receptor gamma (PPAR γ), a member of the NHR superfamily, and a ligand-activated transcription factor that also regulates adipogenesis. It is highly relevant for diabetes control and plays a major role in Type 2 diabetes mellitus development [9–11]. Current PPAR γ -specific antidiabetics, the thiazolidinedione class of drugs such as rosiglitazone and pioglitazone, are full agonists and commonly increase insulin sensitivity. However, they have significant negative side effects, that limit their clinical indications and use [12]. In vitro and in vivo studies both show that FMNT can increase insulin sensitivity and potentially target PPAR γ as a partial agonist [13–16]. FMNT is, therefore, a possible drug candidate that retains insulin sensitization ability without the unwanted side effects associated with full agonism, such as edema and weight gain.

To elucidate the biological role of FMNT, we performed several computational and experimental procedures: (1) single crystal X-ray crystallography to obtain FMNT's molecular structure and information about its intermolecular interactions; (2) determination of FMNT antioxidant activity by measuring its scavenging ability of the superoxide radical; (3) use of computational DFT methods to understand the mechanism of FMNT scavenging of superoxide; (4) characterization of the docking interactions between PPAR γ and FMNT using crystal-structure-obtained FMNT atomic coordinates. Upon observing our FMNT encouraging results, an equivalent analysis of superoxide activity was also performed for three related isoflavones: genistein, daidzein and biochanin A. FMNT and biochanin A are converted by 4'-O-demethylation through cytochrome P-450 enzymes to daidzein and genistein, respectively [17].

2. Results and Discussion

2.1. X-ray Diffraction

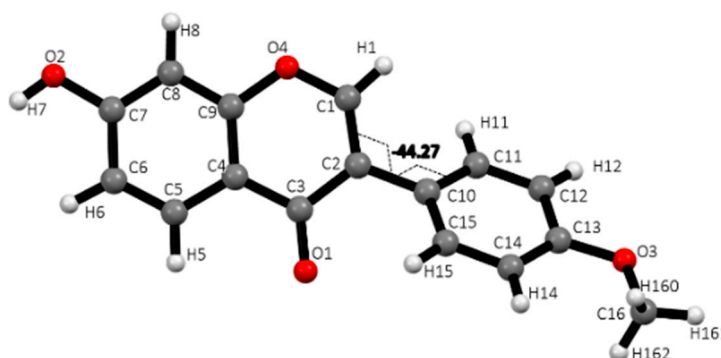
Single crystal X-ray diffraction data obtained on a suitable crystal of FMNT are reported in Table 1. The crystal structure shows hydrogen bonding and stacking interactions intermolecular interactions typical of polyphenolic compounds. Torsion angles show the chromone moiety rings, A and C, are in the same plane, while the exocyclic phenyl ring, designated B, is rotated $-44.3(2)^\circ$ from that plane as seen in Figure 1.

Table 1. Crystal Data for FMNT.

Chemical Formula	C ₁₆ H ₁₂ O ₄
Formula weight	268.26 g/mol
Crystal size	0.020 × 0.110 × 0.220 mm
Crystal color/habit	Yellow/long thin plate
Crystal system	monoclinic
Space group	P2 ₁
Unit cell dimensions	a = 3.7899(5) Å α = 90° b = 13.7156(18) Å β = 96.680(2)° c = 11.9610(16) Å γ = 90°
Volume	617.52(14) Å ³
Z	2
Density (calculated)	1.443 g/cm ³
Absorption coefficient	0.104 mm ⁻¹
F(000)	280
Theta range for data collection	2.27 to 29.06°
Index ranges	$-5 \leq h \leq 5, -18 \leq k \leq 18, -16 \leq l \leq 16$
Reflections collected	14,183
Independent reflections	3307 [R(int) = 0.0557]

Table 1. Cont.

Chemical Formula	C₁₆H₁₂O₄
Coverage of independent reflections	99.9%
Absorption correction	Multi-Scan
Max. and min. transmission	0.9980 and 0.9770
Data/restraints/parameters	3307/1/230
Goodness-of-fit on F ²	1.036
Final R indices	2484 data; I > 2σ(I) R1 = 0.0507, wR2 = 0.1038 all data R1 = 0.0779, wR2 = 0.1167
Weighting scheme	w = 1/[σ ² (F _o ²) + (0.0583P) ² + 0.0556P], where P = (F _o ² + 2F _c ²)/3
Extinction coefficient	0.0050(50)
Largest diff. peak and hole	0.288 and −0.245 eÅ ^{−3}
R.M.S. deviation from mean	0.055 eÅ ^{−3}

**Figure 1.** Single FMNT molecule with atom labeling scheme and showing the -44.3° torsion angle of the twisted (B) phenyl ring.

The FMNT crystal structure shows intermolecular interactions including a strong hydrogen bond (2.649 Å) between carbonyl O1 and hydroxyl group on C7 (Figure 2A). Other interactions listed in Table 2 include CH \cdots O hydrogen bonds, as well as offset stacking interactions of 3.459 Å (Figure 2B).

Table 2. Hydrogen bond distances (Å) and angles ($^\circ$) for the crystal structure of FMNT, described in Figure 2.

	Donor-H	Acceptor-H	Donor-Acceptor	Angle
C1-H1 \cdots O3#3	0.97(4)	2.39(4)	3.282(5)	152.(3)
C6-H6 \cdots O1#2	1.01(4)	2.38(4)	3.158(4)	133.(3)
C12-H12 \cdots O4#1	0.94(4)	2.57(4)	3.472(4)	161.(3)
O2-H7 \cdots O1#2	0.86(6)	1.80(6)	2.649(4)	169.(5)
Symmetry transformations used to generate equivalent atoms:				
#1	$-x, y - 1/2, -z$			
#2	$-x, y + 1/2, -z + 1$			
#3	$-x + 1, y + 1/2, -z$			

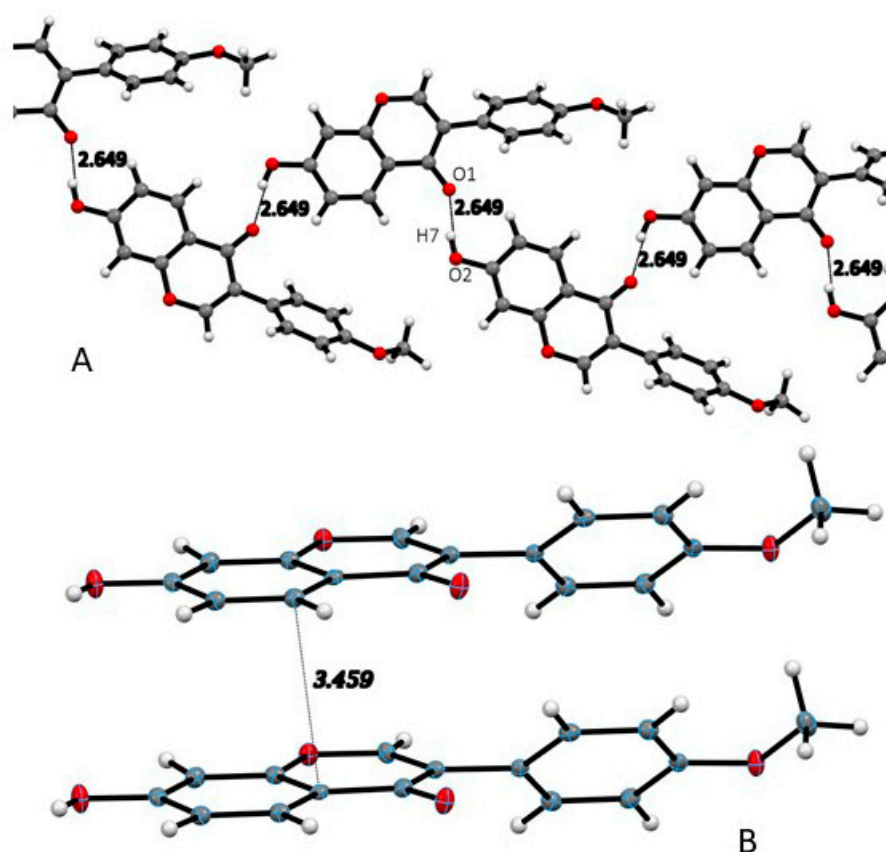


Figure 2. (A) FMNT strong hydrogen bond chain throughout the crystal structure. (B) Intermolecular interactions of offset stacking among FMNT molecules.

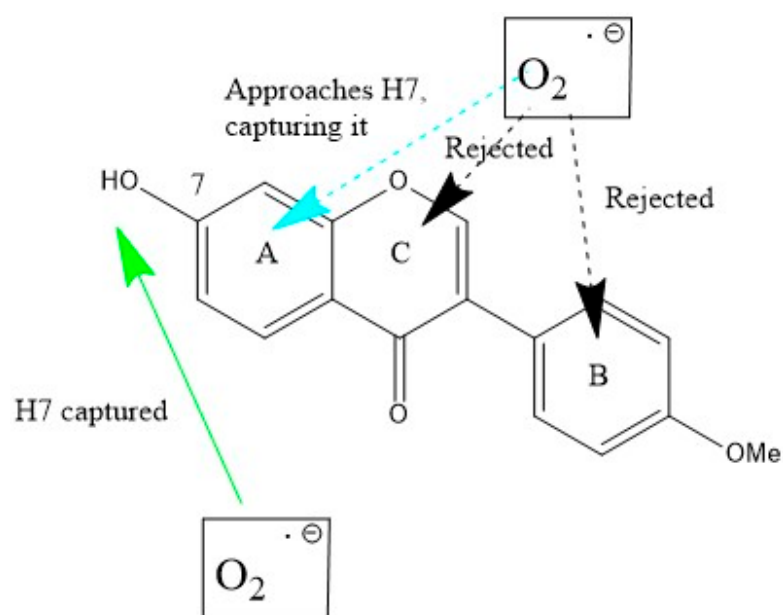
In the Cambridge Structural Database (CSD) [18], there are crystallographic coordinates deposited for genistein (GENIST02), daidzein (XEKCUO) and biochanin A (IHAHIL). Investigation of these related structures shows that all of them have similar torsion angle twists of the exocyclic phenyl ring B with values of 47.71° and -45.92° for the two molecules in the asymmetric unit of biochanin A; 45.06° for daidzein; 54.97° for genistein. All three isoflavones also show offset stacking interactions at distances close to that seen in FMNT (3.453–3.485 Å).

2.2. Computational Antioxidant Activity

2.2.1. FMNT Scavenging

Scavenging of superoxide was analyzed with DFT methods. In a recent review we described two ways of scavenging this radical by polyphenols: (1) superoxide interaction with an aromatic H(hydroxyl) (conventional polyphenol scavenging, that we call σ) and (2) interaction through the π - π approach [19], see Scheme 1.

Scheme 1 shows both scavenging modes for FMNT, which has only one H(hydroxyl) available for σ interaction, at position 7. The initial approach consists of posing one O(superoxide) atom at a van der Waals separation of 2.60 Å from H7, Figure 3A. After DFT geometry minimization, this H atom is captured by the radical to form the anion HO_2^- , while the remaining FMNT polyphenol comprises the unpaired electron located at ring A, Figure 3B. There are three options for π - π interaction, one for each of the A, B and C (pyrone) aromatic rings. The superoxide radical was posed over each ring at a van der Waals separation of 3.50 Å, between superoxide and ring centroids. Upon DFT optimization, the superoxide approaching ring A was directed towards H7, i.e., forming the same pattern shown in the σ attack. This is seen in the deposited Video S1. When acting above rings B and C, the superoxide radical was rejected, as evidenced by final distances of 3.707 Å and 3.563 Å, respectively.



Scheme 1. Formnonetin (FMNT) interactions with superoxide. Bottom (σ attack): H(hydroxyl) in position 7 is captured (green arrow). Top (π attack towards the three ring centers): only ring A is effective (turquoise arrow), and the superoxide radical is directed towards H7, i.e., as when originated from σ scavenging. Interactions with rings B and C result in superoxide rejection.

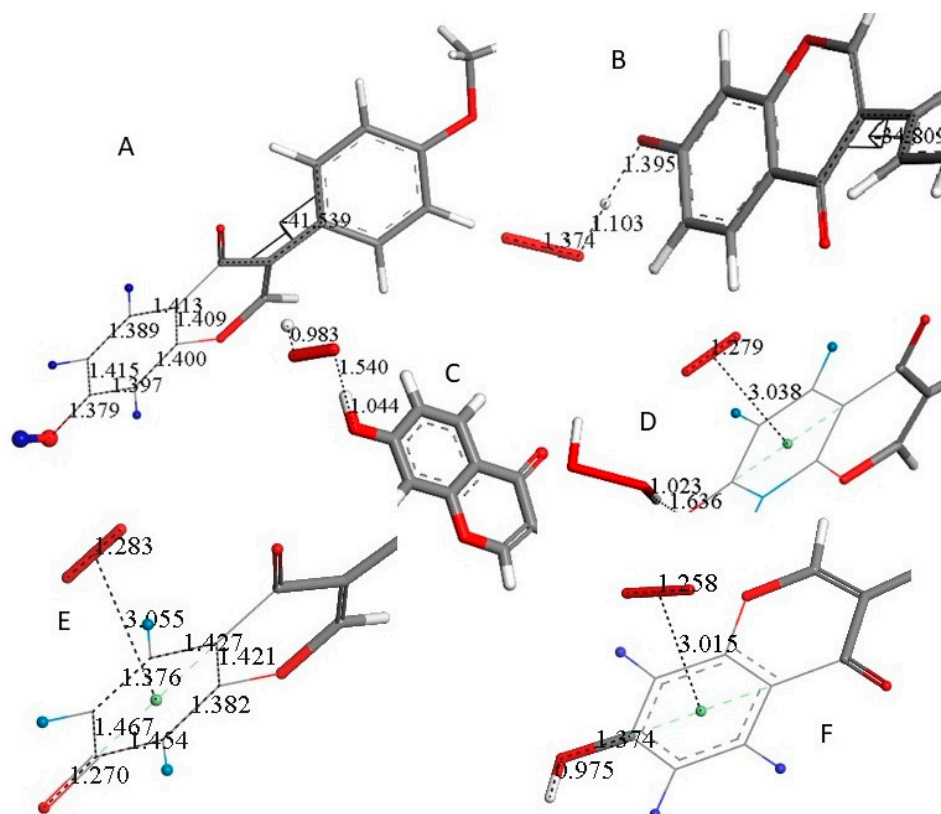
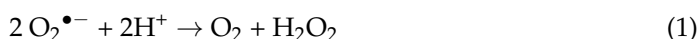


Figure 3. Molecules are truncated to allow larger views, only (A) is complete. (A) DFT minimized molecule of FMNT after the input of X-ray coordinates, a slight variation of the torsion angle, -34.8° , is seen when compared with the X-ray structure, -44.7° . H atoms belonging to ring A are blue. (B) A superoxide was posed 2.60 Å near FMNT H7 and upon DFT minimization H7, it was captured by superoxide, H7-O(superoxide) = 1.103 Å following H atom transfer (HAT). (C) A proton was van der Waals posed near the most exposed O(superoxide) and captured, 0.983 Å. However, O7-H7 is reformed.

1.044 Å. (D) A second superoxide is π - π posed over ring A, and upon DFT this becomes bound to the ring, 3.038 Å, while H₂O₂ is formed and well separated, 1.636 Å, from the remaining polyphenol. Calculation in DMSO solvent shows a slightly longer separation between centroids, 3.043 Å. The difference of energy between the reagent and product in the gas phase is −41.9 Kcal/mol. (E) After H₂O₂ is eliminated, DFT shows still the second superoxide trapped by ring A, with a distance of 3.055 Å between both centroids, shorter than the 3.50 van der Waals separation. (F) A proton is posed by O7, and upon DFT minimization O7-H7 is formed, 0.975 Å. This is a neutral molecule that still comprises the π - π bound second superoxide.

Scavenging details after the capture of H7 by superoxide FMNT are shown in Figure 3. Figure 3A shows the result after DFT minimization of X-ray FMNT coordinates, and a slight variation in the torsion angle between rings B and C is observed, −34.8° (DFT) and −44.7° (X-ray). Figure 3B shows the result of posing a van der Waals separated (2.60 Å) superoxide radical near H7; upon DFT minimization, H7 is captured with the formation of HO₂[−], separated 1.395 Å from O(7). When a proton is van der Waals posed near the more exposed O(superoxide) moiety, DFT minimization shows bond formation, O-H distance = 0.983 Å, while HO₂[−] is separated by 1.540 Å from the polyphenol. However, H7 results as returning to FMNT, O7-H7 = 1.044 Å, Figure 3C. This resonance stabilization through the phenolic ring A allows inclusion of the unpaired superoxide electron. From the configuration shown in Figure 3C, a second superoxide was placed over of ring A for π - π interaction at a van der Waals separation of 3.50 Å. At this point, the charge of the whole system is −1, due to two superoxide anion radicals plus one proton. Upon DFT minimization, H₂O₂ was formed and became well separated from ring A, 1.636 Å, while the stacked superoxide reagent became trapped within the ring, with a separation between centroids of 3.038 Å, which is shorter than the original van der Waals separation of 3.50 Å, Figure 3D. Hence, H₂O₂ was eliminated and upon DFT minimization, Figure 3E shows a partial double bond formation with a C7-O7 distance of 1.270 Å, which can be compared to the corresponding initial longer single bond moiety in FMNT, 1.379 Å, Figure 3A. Further comparison of Figure 3E with Figure 3A indicates that strong localization in ring A took place as C5-C6 (1.376 Å) and C8-C9 (1.382 Å) bonds are shorter than conjugated adjacent bonds, 1.427 Å, 1.421 Å, 1.454 Å and 1.467 Å. This alternating pattern of single–double bonds has been observed previously in related polyphenols after scavenging superoxide [20]. From the structure shown in Figure 3E, a proton was van der Waals posed near O7, and upon DFT optimization, FMNT reformed. However, the π - π interacting O₂ molecule (O-O bond length of 1.258 Å) is still bound to ring A, as shown by a centroid separation of 3.015 Å, Figure 3F.

Next, we explored if this FMNT- η -O₂ complex could behave as a catalyst for superoxide scavenging, i.e., beginning a new cycle. Another superoxide radical was σ van der Waals posed (2.60 Å) near H7, and DFT minimization (stopped after 81 cycles) showed initial formation of HO₂[−] ion, separated from FMNT 1.717 Å. More importantly, the π - π superoxide inserted in Figure 3D was rejected at a distance of 5.729 Å. Indeed, the latter is a molecule of O₂, as shown by its O-O bond distance of 1.289 Å, which is much shorter than 1.373 Å for the superoxide. Thus, Figure 4 is formally equivalent to Figure 3A and confirms that FMNT can perform cyclic scavenging by consuming two superoxides, Figure 3B,D, plus two protons, Figure 3C,E, while giving H₂O₂, Figure 3D, and O₂ Figure 4. This reaction (1) is the same as performed by superoxide dismutases (SOD), a family of metalloenzymes used to counteract excessive superoxide in cells [21,22]. Scheme 2 shows the whole process of scavenging superoxide by FMNT.



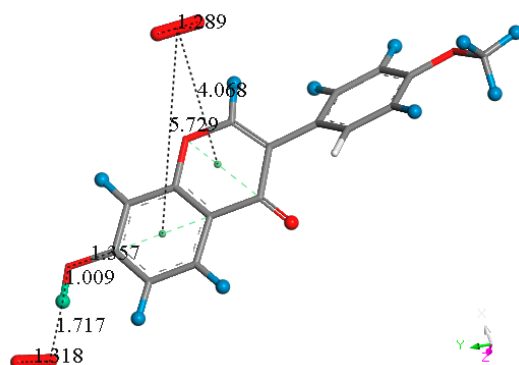
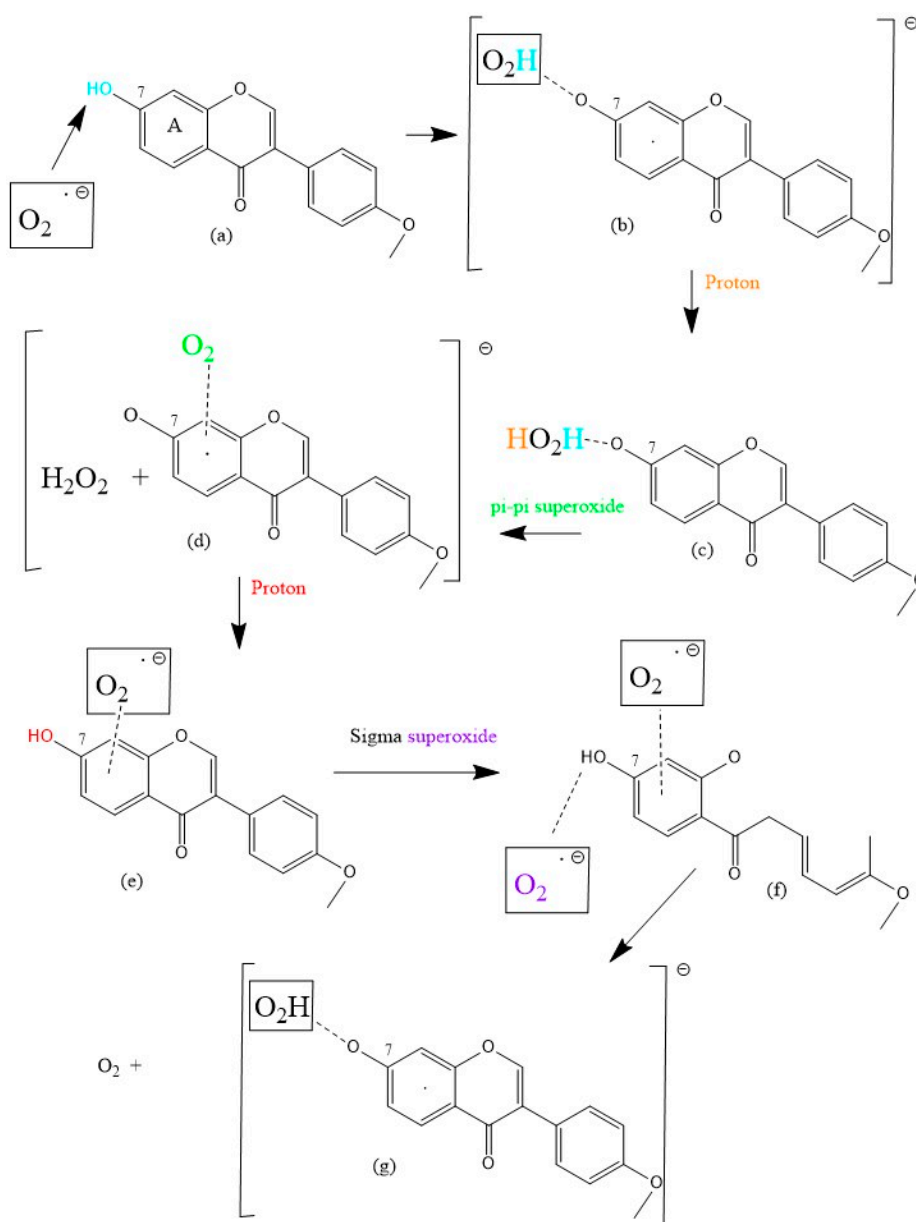


Figure 4. After approaching an additional superoxide of σ type close to H7, the π - π bound original superoxide, separated 3.015 Å from ring A (Figure 3F), is expelled from the polyphenol, 5.729 Å, as shown by this unfinished geometry optimization, and FMNT is reformed. It will be shown later that in the equivalent situation genistein behaves differently regarding ring C.

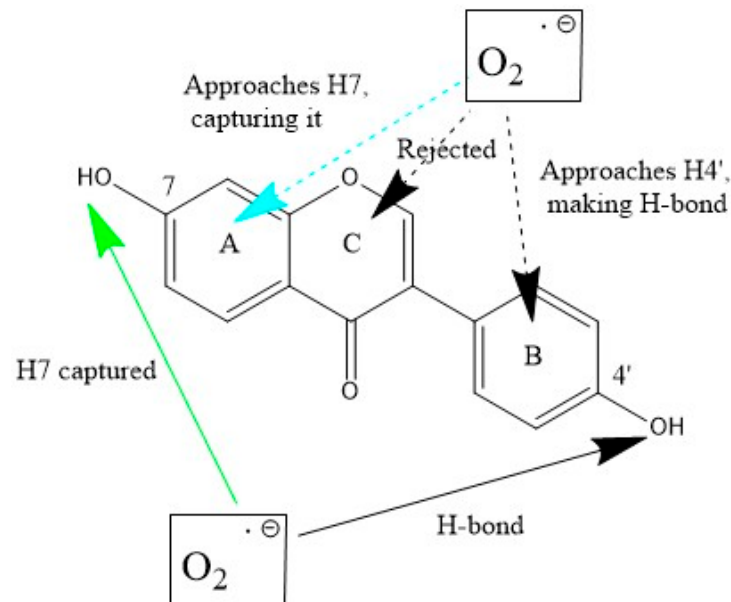


(B) HO_2^- was posed near a proton and DFT minimization showed H_2O_2 formation, separated 1.621 Å from O7, not shown, then a second superoxide was π - π posed on top of the A ring, with a separation of 3.50 Å between their centroids. Upon DFT minimization, the centroid separation shortened slightly by 3.477 Å, the superoxide O-O bond length became similar to that in the molecule of O_2 , 1.276 Å, i.e., suggesting transfer of the superoxide electron to the polyphenol. Meanwhile, O7-H7 became closer, 1.573 Å. (C) After the elimination of H_2O_2 in B, a proton was posed near O7, 2.60 Å, and minimization resulted in restoring the genistein O7-H7 bond. This also strengthened the penetration of O_2 in the ring environment, 2.931 Å. (D) After an additional superoxide was σ type posed to H7, DFT shows the π - π bound molecule of O_2 leaving ring A, 4.398 Å, and relocating above ring C, i.e., having both centroids separated by 3.154 Å. This structure differs from the equivalent one shown in Figure 4, where the molecule of O_2 was completely displaced from FMNT.

Figure 5A shows the σ attack on H7. Contrary to FMNT, when a proton interacts with the exposed O(superoxide) moiety of genistein-H7- O_2 , H_2O_2 forms and is well separated from genistein's radical, 1.621 Å, which is not shown. Figure 5B shows the DFT minimization after superoxide is π - π added onto ring C. Figure 5C shows results from eliminating H_2O_2 and posing a proton near O7. Proceeding in a similar way as with FMNT, the additional superoxide posed near H7 induces the π - π molecule of O_2 to leave, not shown, while the last superoxide forms a H-bond to H7. Meanwhile the second superoxide relocates above ring C, 3.154 Å, between centroids, Figure 5D. Thus, genistein behaves as FMNT and is able to perform another scavenging cycle, mimicking SOD action.

2.2.3. Daidzein Scavenging

Scheme 4 shows σ and π - π interactions between the superoxide and daidzein.



Scheme 4. Daidzein interactions with superoxide. Bottom (σ attack): H(hydroxyl) in position 7 is captured (green arrow). When directed towards H4' superoxide a H-bond is established. Top (π attack towards the three ring centers): when ring A is approached, the superoxide radical is later directed towards H7 (turquoise arrow), which is captured, i.e., as when originated from σ -scavenging. Interactions with rings C results in superoxide rejection, whereas when initially directed towards ring B, the superoxide behaves as its equivalent σ approach towards H4' that is forming a H-bond.

Daidzein behavior is similar to that of FMNT and genistein. Figure 6A shows the initial π - π attack of superoxide on ring A, which is equivalent to the previously described FMNT σ -scavenging on H7 that then forms HO_2^- . Next, a proton was posed near the

most exposed O(HO₂⁻) and DFT minimization resulted in H₂O₂ formation. Upon H₂O₂ elimination, a π - π superoxide was posed over ring A and DFT was applied resulting in the superoxide being released as a molecule of O₂, Figure 6C. Finally, a proton was van der Waals posed near O7 and DFT calculations showed reformation of daidzein. In summary, daidzein is able to consume two superoxides, Figure 6A,C, plus two protons, one shown in Figure 6B, and the other in the process explained in Figure 6C, whereas H₂O₂ is eliminated after Figure 6B, and O₂ is released after the final proton is incorporated in Figure 6C. Thus, daidzein, FMNT and genistein, are polyphenols able to act as SOD mimics.

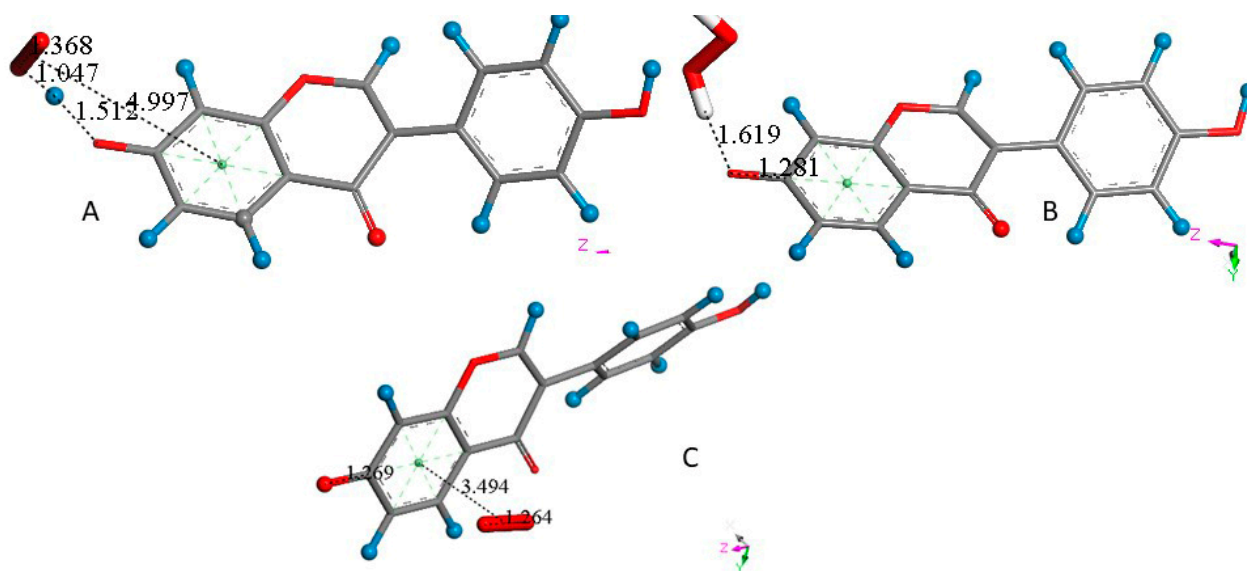
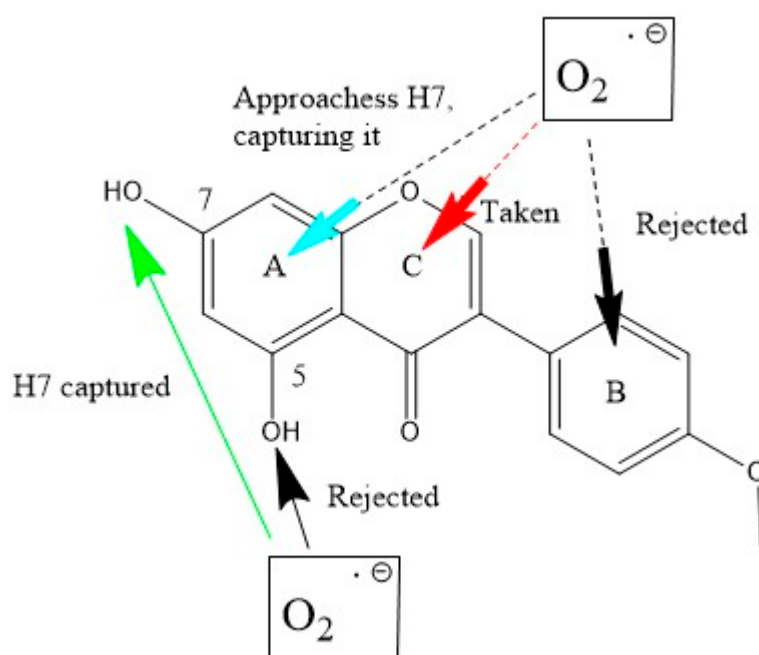


Figure 6. (A) The π - π interaction between superoxide and daidzein ring A results in the same arrangement as that seen performing a σ interaction, i.e., the original separation between superoxide and ring A centroids, 3.50 Å, becomes 4.997 Å, while H7 is captured by superoxide (following an H atom transfer (HAT)), O(superoxide-H7) = 1.047 Å (1.069 Å in DMSO solvent), and HO₂⁻ forms, well separated from O7, 1.512 Å (1.445 Å in DMSO). The difference of energy between the reagent and product in the gas phase is -181.7 Kcal/mol. (B) After posing the more exposed oxygen atom of HO₂⁻ near a proton, DFT minimization shows H₂O₂ formation, well separated from O7, 1.619 Å. (C) After elimination of H₂O₂ and posing a π - π superoxide over ring A, DFT minimization shows the formation of O₂, seen by an O-O bond length of 1.264 Å, separated by 3.494 Å from ring A centroid, i.e., the superoxide electron has been transferred to the polyphenol system. Therefore, after posing a proton 2.60 Å near O7 and applying DFT minimization, a molecule of O₂ results in being eliminated and daidzein becomes reformed ready for performing another SOD cycle, not shown.

2.2.4. Biochanin A Scavenging

Scheme 5 shows biochanin A results, where H7 is again σ scavenged. The π - π scavenging shows ring B rejection of superoxide and the formation of biochanin A- η -O₂ complex with ring C centroid, 2.844 Å, as is the case with genistein, whereas the attack on ring A occurs as a σ scavenging on H7.

The biochanin A path of scavenging is similar to that of the other three isoflavones. First, H7 is well captured by superoxide, following an H atom transfer (HAT), both through σ or π - π approaches. Next, a proton was added, and upon DFT minimization, a well separated H₂O₂ moiety was seen, 1.621 Å from the remaining biochanin neutral radical. Hence, H₂O₂ was eliminated, the biochanin A radical was minimized and another proton was posed near O7. Upon DFT minimization, O7-H7 formed, and additional superoxide was a van der Waals π - π posed on ring A, 3.50 Å. The subsequent DFT minimized structure is the real catalyst for biochanin A mimicking SOD action, Figure 7.



Scheme 5. Biochanin A interactions with superoxide. Bottom (σ attack): H7(hydroxyl) is scavenged (green arrow), whereas H(hydroxyl) in position 5 is rejected. Top (π attack with the three ring centers): when interacting with ring A, H7 is captured (turquoise arrow), as was the case for σ scavenging. With ring C, the formation of a π - π biochanin- η - O_2 complex is established, i.e., the separation between both centroids is shorter than the van der Waals distance of 3.50 Å (red arrow), 2.844 Å. With ring B, there is the rejection of superoxide.

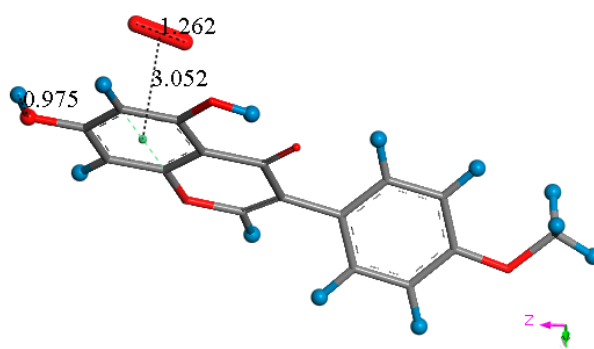


Figure 7. Biochanin A is reformed after acting like SOD, and includes a π - π bound molecule of O_2 . This O_2 - η -biochanin complex is able to initiate another cycle of scavenging superoxide. This structure is closely related to that shown in Figure 3F.

2.3. Structural Details When the π - π Approach Is First Performed

As mentioned earlier, when the superoxide resides above ring A, the response of the four isoflavones is the same: the superoxide radical is redirected to H7 that is then captured, as shown in deposited Video S1 for FMNT. In contrast, there are differences in superoxide approaching the other two rings B and C. Thus, FMNT and biochanin A show rejection of the superoxide, whereas for genistein and daidzein, the superoxide is redirected towards the 4'-hydroxyl located in ring B, forming a H-bond. This is obviously not possible for FMNT and biochanin as they have a methoxy group in position 4'. The H-bond between superoxide and H4'(hydroxyl) is also formed after a π - π approach over ring B for genistein and daidzein. Interestingly, a superoxide π - π approach over the pyrone ring C results in a bond with genistein and biochanin being established, but not for FMNT and daidzein; the reason for this difference is not obvious. The difference in energy between reagents

and products for the O₂-η-biochanin-A complex, Figure 7, is −178.0 Kcal/mol, and for the equivalent O₂-η-genistein, it is −147.7 Kcal/mol. Table 3 lists all possibilities of π–π interactions, with related structural parameters.

Table 3. Converged structures after DFT geometry optimization for superoxide and polyphenols π–π van der Waals distance initial separation, 3.50 Å. The difference in energy between the reagent and product is −157.7 Kcal/mol (genistein) and −178.0 Kcal/mol (biochanin A). * Calculation in DMSO solvent shows a slightly longer separation between the inserted superoxide and ring C centroids.

	Ring A		Ring B		Ring C	
	Centroid Separation	O-O Bond Length	Centroid Separation	O-O Bond Length	Centroid Separation	O-O Bond Length
FMNT	Longer than 3.50; H7 capture	1.369	Rejection		Rejection	
Genistein	Longer than 3.50; H7 capture	1.369	Longer than 3.50; H-bond to H4'	1.333	3.030 (* 3.102)	1.327 (* 1.344)
Daidzein	Longer than 3.50; H7 capture	1.368	Longer than 3.50; H-bond to H4'	1.269	Rejection	
Biochanin A	Longer than 3.50; H7 capture	1.377	Rejection		2.844 (* 2.979)	1.321 (* 1.349)

2.4. Hydrodynamic Cyclovoltammetry

The DFT scavenging activity of the four isoflavones was measured using a previously established cyclic voltammetry protocol [23]. This method uses a rotating ring disk electrode (RRDE) method that confirms and quantifies the antioxidant activity. Figures 8–11 show the corresponding results for the four isoflavones in this study.

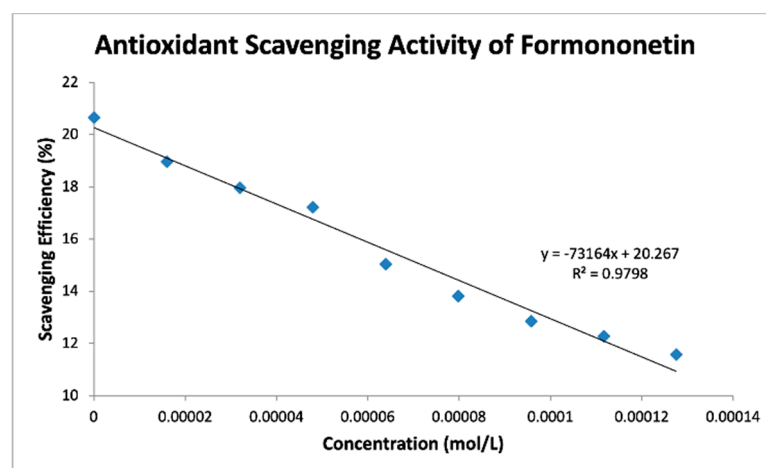


Figure 8. FMNT scavenges superoxide radicals in DMSO solution.

Table 4 shows slopes of Collection Efficiency (indicators of scavenging superoxide) [8] for several polyphenols using the RRDE method in the literature. The four isoflavones in the present study have slopes in between eriodictyol and butein (FMNT: -7.3×10^4 ; genistein: -6.4×10^4 ; daidzein: -7.0×10^4 ; biochanin A: -7.1×10^4). They are slightly weaker than DHDM, 2',4'-dihydroxy-3,4-dimethoxy chalcone, which contains a 2',4'-dihydroxy ring moiety responsible for scavenging. Butein, clovamide and quercetin are stronger scavengers than the isoflavones in this study and have catechol moieties, a structural feature associated with good scavenging activity. However, the best superoxide scavenger so far studied by the RRDE technique, galangin, has no ring B-hydroxyls.

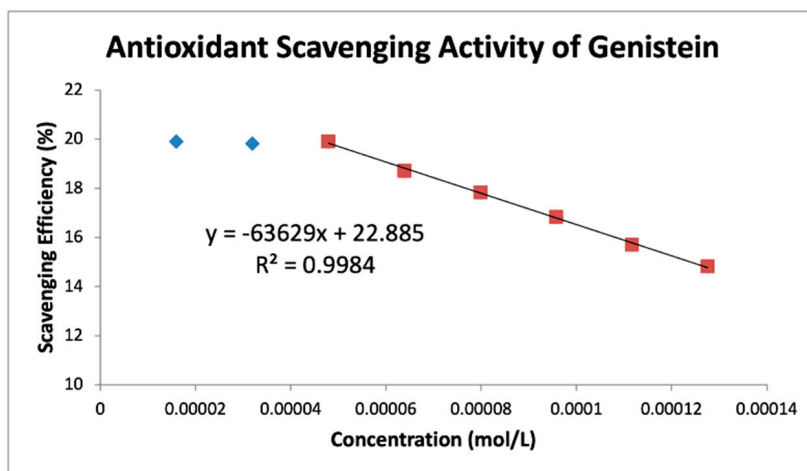


Figure 9. Genistein RRDE scavenging efficiency. The first two aliquots were not effective in scavenging superoxide and were omitted for line calculation.

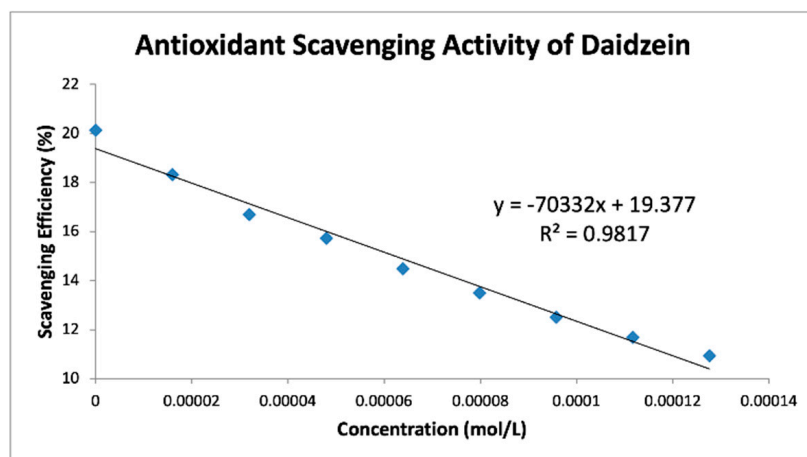


Figure 10. Daidzein RRDE cyclic voltammetry collection efficiency.

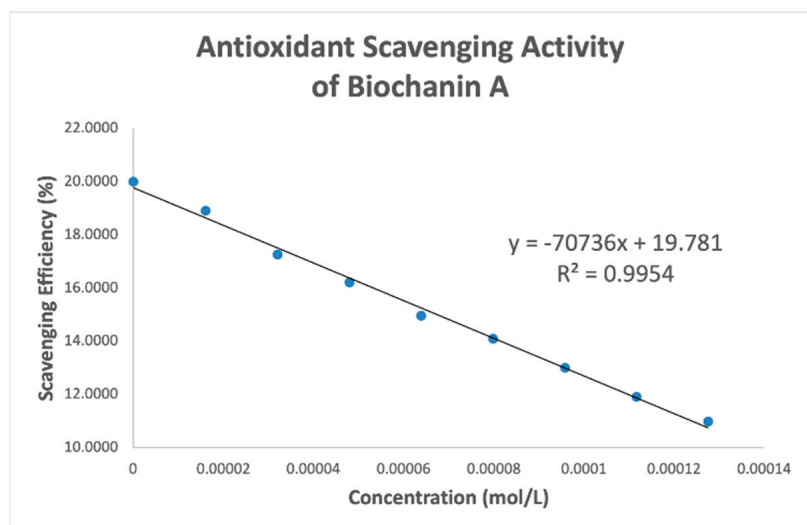


Figure 11. Biochanin collection efficiency.

Table 4. Slopes of several polyphenols analyzed with the RRDE method.

BHT	Chrysin	Eriodictyol	DHDM	Butein	Clovamide	Quercetin	Galangin
-0.16×10^4 [24]	-1.10×10^4 [23]	-2.20×10^4 [23]	-8.0×10^4 [25]	-11.2×10^4 [25]	-12.0×10^4 [26]	-15.5×10^4 [23]	-19.0×10^4 [20]

2.5. FMNT Docking into the PPAR γ Ligand Binding Domain (LBD)

To better understand the interactions of FMNT as a possible PPAR γ partial agonist, atomic coordinates from the crystal structure of FMNT were docked in the PPAR γ ligand binding domain (LBD), PDB Code: 5UGM [27], which contains edaglitazone in the active site. After applying CHARMM force field, the protocol “prepare protein” was applied to also provide H atoms to the protein. The edaglitazone position at the active site was selected to define the sphere of radius 10 Å and later eliminated. Docking of FMNT in this PPAR γ LBD was affected for 10 poses and showed Cys285 π -interactions with FMNT rings. Pose 5 and pose 4 formed a cluster that was selected for further calculations, which included a standard dynamic cascade. The latter calculation confirmed Cys285 π -bonded to ring A (2.521 Å) and strengthened its interaction by the pyrone ring centroid, 2.758 Å (Figure 12). Initially, these were 2.569 Å and 3.110 Å, respectively, at docking. The environment of FMNT includes van der Waals interactions with Arg288 and Ile341 amino acids, Figure 13. Previous work has established that nearly every partial agonist interacts in a hydrophobic manner with Cys285 of Helix 3 and most interact with Arg288 using either electrostatic interactions or hydrophobic interactions. However, partial agonists that lack an acidic group can also stabilize the β -sheet by means of hydrophobic interactions, especially with the side chain of Ile341 [16]. These three amino acids show a similar role in our docking study, thus suggesting FMNT for potential use as partial agonist of PPAR γ domain. Figure S3 displays a partial view of the 5UGM protein, including FMNT pose 5 “Calculating Binding Energy” after standard dynamic cascade.

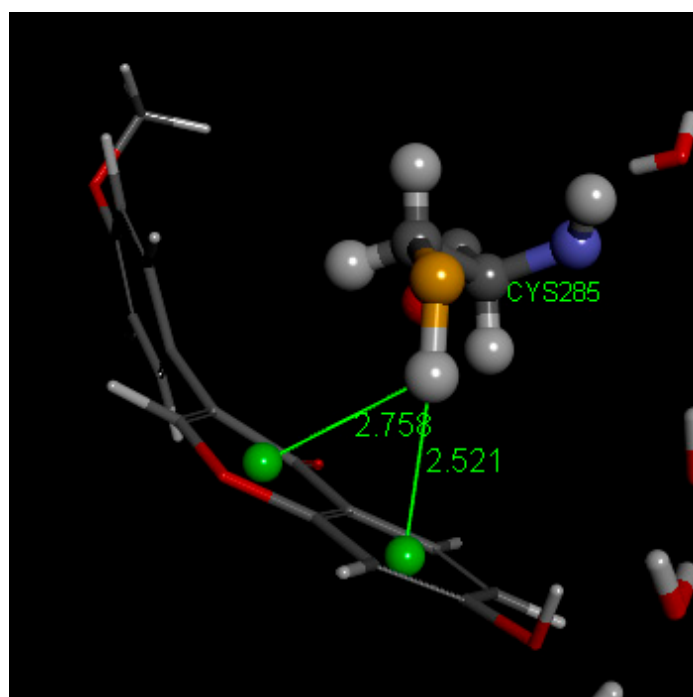


Figure 12. Standard dynamic cascade shows Cys285 forming a strong π -alkyl bond with FMNT’s pyrone and A rings. FMNT forms a sort of basket arrangement at the active site.

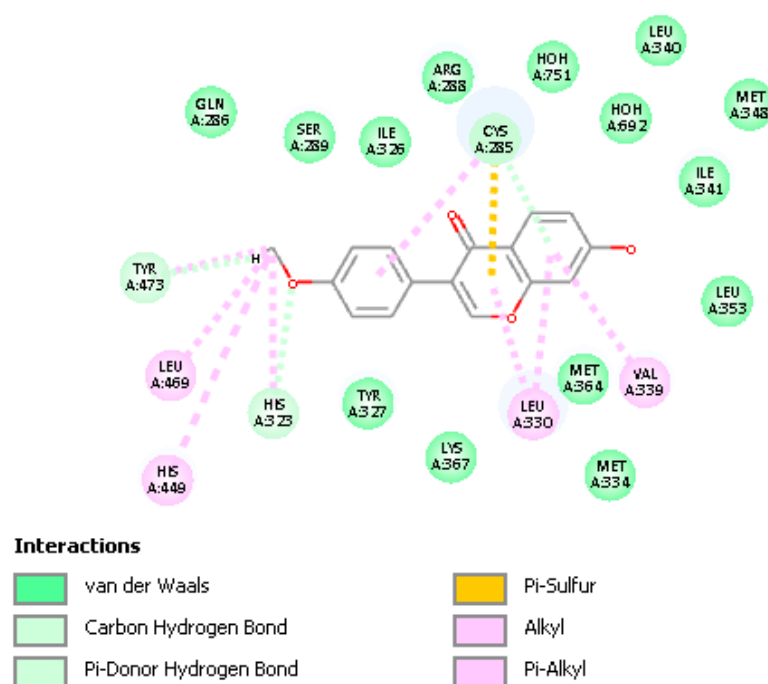


Figure 13. Dynamics calculation of FMNT shows its stabilization in the ligand-binding pocket by a combination of van der Waals interactions and π -alkyl bonds, including the important amino acids Cys285, Arg288 and Ile341.

3. Materials and Methods

3.1. X-ray Structures

Formononetin was recrystallized from ethanol by slow evaporation. An APEX2 DUO platform X-ray diffractometer from Bruker Advanced X-ray Solutions was used to obtain X-ray data measurements at 125 K. Temperature was maintained using a cold liquid nitrogen stream from Oxford cryosystems; the X-ray source emitted MoK α radiation at 0.71069 Å. The crystal structure was solved and refined using full-matrix least-squares on F^2 with the Bruker incorporated ShelX programs [28]. We input the X-ray data into the MERCURY program from Cambridge Structural Database (CSD) to produce images of the molecules and crystal packing [29]. Crystal data of FMNT have been deposited at the CSD and are available at <https://www.ccdc.cam.ac.uk/structures/> (accessed on 28 October 2022) using Identifier CCDC number 2216211.

3.2. RRDE Measurement of Antioxidant Activity

Materials used to determine the antioxidant activity of the 4 isoflavones were tetrabutylammonium bromide (TBAB; Sigma Aldrich, St. Louis, MO, USA) and 99.9% anhydrous dimethyl sulfoxide (DMSO; Sigma Aldrich). The four isoflavones, FMNT, genistein, daidzein and biochanin A, were all obtained from Indofine Chemical Company (Hillsborough, NJ, USA). A 0.1 M TBAB/DMSO solution was used to produce electric current and enhance the occurrence of redox reactions. Antioxidant activity was measured via the hydrodynamic voltammetry technique with a rotating ring disk electrode (RRDE). The equipment used in this experiment was an MSR electrode rotator together with a WaveDriver 20 benchtop USB from Pine Instrumentation, Grove City, PA, USA. The main electrode tip was an E6RI ChangeDisk with a rigid gold ring and gold disk (Au/Au) insert. Before and after each experiment, 0.5 μ m alumina suspension was used to clean the disk electrode tip (Allied High Tech Products, Inc., Rancho Dominguez, CA, USA) on a moistened polishing microcloth to eliminate potential film formation. A platinum (Pt) reference electrode and Pt counter electrode were also used in this experiment. All electrodes were obtained from Pine Research, Durham, NC, USA [30]. Cyclic voltammograms were run using a Solartron SI 1287 Potentiostat/galvanostat (Solartron Analytical, Oakridge, TN, USA) controlled through

Coreware[®] software. The antioxidant activity of the four isoflavones (all of them 99.9% pure) was determined based on their superoxide radical scavenging ability that was measured using the protocol developed in our lab [23]. Stock solutions of all compounds (99.9% purity) were prepared. Biochanin A, MW = 284.27, 0.071 g dissolved in 5 mL of DMSO, concentration = 0.05 M; genistein, MW = 270.25, 0.054g/4 mL DMSO, concentration = 0.05 M; formononetin, MW = 268.27, 0.107g/8 mL DMSO, concentration = 0.05 M; daidzein, MW = 254.24, 0.081 g/8 mL DMSO; concentration = 0.05 M.

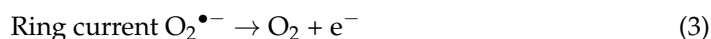
For the experiment, the electrolytic cell was bubbled for 5 min with a dry O₂/N₂ (35%/65%) gas mixture to establish its dissolved oxygen level. The Au disk electrode was then rotated at 1000 rpm while the disk was swept from 0.2 V to −1.2 Volts and the ring was held constant at 0.0 Volts, the disk voltage sweep rate was set to 25 mV/s. Several runs plus blank were performed in the RRDE experiment for the 4 compounds to determine their antioxidant activity with equal addition of 5 μL of each stock solution.

Results from each run were collected on Aftermath software and represented as voltammograms showing current vs. potential graphs that were later analyzed using Microsoft Excel. In an RRDE voltammetry experiment, the generation of the superoxide radicals occurs at the disk electrode while the oxidation of the residual superoxide radicals (that have not been scavenged by the scavenger) occurs at the ring electrode.

Reaction 2: Reduction of molecular oxygen at the disk electrode



Reverse Reaction 3: Oxidation of superoxide radicals at the ring electrode



Thus, the rate at which increasing concentrations of antioxidant scavenged the generated superoxide radicals during the electrolytic reaction was determined by obtaining the ring current/disk current (percent value) at each concentration. These values were denoted as the Efficiency of the scavenger at different concentrations. Using Microsoft Excel, Collection Efficiency values were plotted against the corresponding concentrations of each analyzed compound to produce a graph illustrating the effect of their increasing concentrations on the scavenging of superoxide radicals in the electrolytic solution. Ultimately, the slope of the curves served as a quantitative measure of the antioxidant activity of each compound.

3.3. Theoretical Calculations: Isoflavones Studied Using DFT and Molecular Mechanics

Calculations were performed using programs from Biovia (San Diego, CA, USA). Density functional theory (DFT) program DMol3 was applied to calculate energy, geometry and frequencies implemented in Materials Studio 7.0 [31]. We employed the double numerical polarized (DNP) basis set that included all the occupied atomic orbitals plus a second set of valence atomic orbitals, and polarized d-valence orbitals [32]; the correlation generalized gradient approximation (GGA) was applied including Becke exchange [33], plus BLYP correlation including Grimme's correction when van der Waals interactions were involved [34]. All electrons were treated explicitly and the real space cutoff of 5 Å was imposed for numerical integration of the Hamiltonian matrix elements. The self-consistent field convergence criterion was set to the root mean square change in the electronic density to be less than 10^{−6} electron/Å³. The convergence criteria applied during geometry optimization were 2.72 × 10^{−4} eV for energy and 0.054 eV/Å for force. Calculations were generally performed with no solvent inclusion, those made in DMSO are specifically indicated. Docking studies were performed with the CDocker package in Discovery Studio 2020 version [35].

4. Conclusions

The X-ray structure presents FMNT's ability to have strong intermolecular interactions, such as hydrogen bonding and stacking, which are useful for antioxidant actions. Antioxidant activity measured using the RRDE method revealed the four isoflavones to share a similar pattern in the collection efficiency slopes. All DFT calculations confirm these findings and allow us to conclude that antioxidant activity is based on the familiar superoxide σ -scavenging mode involving ring-A H7(hydroxyl) capture and supplemented by the π - π (polyphenol-superoxide) scavenging activity. These results suggest the possibility of their mimicking SOD action and help to explain the ability of natural polyphenols to assist in lowering superoxide concentrations. The SOD metalloenzymes all dismutate $O_2^{\bullet-}$ to H_2O_2 plus O_2 through metal ion redox chemistry [21], whereas these polyphenolic compounds do so through suitable intermolecular interactions (hydrogen bonding and stacking interactions). This theoretical assessment is confirmed using the cyclic voltammetry technique of rotating ring disk electrochemistry (RRDE), which results in very similar antioxidant activity for the four isoflavone scavengers, as shown by slopes in collection efficiency. Additionally, docking calculations suggest that FMNT can be a partial antagonist of the PPAR γ domain. Our work shows the efficacy in combining multidisciplinary approaches, including experimental X-ray crystallography and RRDE, as well as computational docking and DFT methods, to provide an understanding of the mechanism of action of small molecule polyphenolic antioxidants. Finally, our findings promote the further exploration of other natural products, including those known to be effective in traditional Chinese medicine for potential drug design in diabetes research.

Supplementary Materials: The following supporting information can be downloaded at: <https://www.mdpi.com/article/10.3390/ijms24043815/s1>.

Author Contributions: Conceptualization, F.C. and M.R.; methodology, S.B. and F.C.; formal analysis, S.Y. and M.R.; data curation, M.R., S.Y. and S.B.; project administration, M.R.; writing original draft preparation, F.C. and M.R.; writing—review and editing, F.C., M.R. and S.B. All authors have read and agreed to the published version of the manuscript.

Funding: This research received no external funding.

Data Availability Statement: Crystal data of FMNT have been deposited at the Cambridge Structural Database (CSD) and are available at <https://www.ccdc.cam.ac.uk/structures/> (accessed on 28 October 2022) using Identifier CCDC number 2216211.

Acknowledgments: We are grateful to the CIS department at Vassar College for computational resources and to Karly Andreassen for computational support. The X-ray diffractometer was obtained using NSF Grant Number 051237 (MR). We thank Sarjit Kaur for helpful conversations.

Conflicts of Interest: The authors declare no conflict of interest.

References

1. Křížová, L.; Dadáková, K.; Kašparovská, J.; Kašparovský, T. Isoflavones. *Molecules* **2019**, *24*, 1076. [[CrossRef](#)] [[PubMed](#)]
2. Popa, D.; Rusu, M.E. Isoflavones: Vegetable Sources, Biological Activity, and Analytical Methods for Their Assessment. In *Superfood and Functional Food—The Development of Superfoods and Their Roles as Medicine*; Shiomi, N., Waisundara, V., Eds.; IntechOpen: London, UK, 2017. [[CrossRef](#)]
3. Zhang, J.; Du, F.; Peng, B.; Lu, R.; Gao, H.; Zhou, Z. Structure, electronic properties, and radical scavenging mechanisms of daidzein, genistein, formononetin, and biochanin A: A density functional study. *J. Mol. Struct. THEOCHEM* **2010**, *955*, 1–6. [[CrossRef](#)]
4. Mu, H.; Bai, Y.-H.; Wang, S.-T.; Zhu, Z.-M.; Zhang, Y.-W. Research on antioxidant effects and estrogenic effect of formononetin from red clover). *Phytomedicine* **2009**, *16*, 314–319. [[CrossRef](#)]
5. Machado Dutra, J.; Espitia, P.J.P.; Andrade Batista, R. Formononetin: Biological effects and uses—A review. *Food Chem.* **2021**, *359*, 129975. [[CrossRef](#)] [[PubMed](#)]
6. Luo, L.Y.; Fan, M.X.; Zhao, H.Y.; Li, M.X.; Wu, X.; Gao, W.Y. Pharmacokinetics and Bioavailability of the Isoflavones Formononetin and Ononin and Their in Vitro Absorption in Ussing Chamber and Caco-2 Cell Models. *J. Agric. Food Chem.* **2018**, *66*, 2917–2924. [[CrossRef](#)] [[PubMed](#)]

7. Tian, H.; Lu, J.; He, H.; Zhang, L.; Dong, Y.; Yao, H.; Feng, W.; Wang, S. The effect of Astragalus as an adjuvant treatment in type 2 diabetes mellitus: A (preliminary) meta-analysis. *J. Ethnopharmacol.* **2016**, *191*, 206–215. [[CrossRef](#)] [[PubMed](#)]
8. Sun, H.; Saeedi, P.; Karuranga, S.; Pinkepank, M.; Ogurtsova, K.; Duncan, B.B.; Stein, C.; Basit, A.; Chan, J.C.N.; Mbanya, J.C.; et al. IDF Diabetes Atlas: Global, regional and country-level diabetes prevalence estimates for 2021 and projections for 2045. *Diabetes Res. Clin. Pract.* **2022**, *183*, 109119. [[CrossRef](#)] [[PubMed](#)]
9. Chandra, M.; Miriyala, S.; Panchatcharam, M. PPAR γ and Its Role in Cardiovascular Diseases. *PPAR Res.* **2017**, *2017*, 1–10. [[CrossRef](#)] [[PubMed](#)]
10. Sarhangi, N.; Sharifi, F.; Hashemian, L.; Hassani Doabsari, M.; Heshmatzad, K.; Rahbaran, M.; Jamaldini, S.H.; Aghaei Meybodi, H.R.; Hasanzad, M. PPARG (Pro12Ala) genetic variant and risk of T2DM: A systematic review and meta-analysis. *Sci. Rep.* **2020**, *10*, 12764. [[CrossRef](#)]
11. Frkic, R.L.; Richter, K.; Bruning, J.B. The therapeutic potential of inhibiting PPAR γ phosphorylation to treat type 2 diabetes. *J. Biol. Chem.* **2021**, *297*, 101030. [[CrossRef](#)] [[PubMed](#)]
12. Diamant, M.; Heine, R.J. Thiazolidinediones in type 2 diabetes mellitus: Current clinical evidence. *Drugs* **2003**, *63*, 1373–1405. [[CrossRef](#)] [[PubMed](#)]
13. Oza, M.J.; Kulkarni, Y.A. Formononetin Treatment in Type 2 Diabetic Rats Reduces Insulin Resistance and Hyperglycemia. *Front. Pharmacol.* **2018**, *9*, 739. [[CrossRef](#)]
14. Nie, T.; Zhao, S.; Mao, L.; Yang, Y.; Sun, W.; Lin, X.; Liu, S.; Li, K.; Sun, Y.; Li, P.; et al. The natural compound, formononetin, extracted from *Astragalus membranaceus* increases adipocyte thermogenesis by modulating PPAR γ activity. *Br. J. Pharmacol.* **2018**, *175*, 1439–1450. [[CrossRef](#)] [[PubMed](#)]
15. Shen, P.; Liu, M.H.; Ng, T.Y.; Chan, Y.H.; Yong, E.L. Differential effects of isoflavones, from *Astragalus membranaceus* and *Pueraria thomsonii*, on the activation of PPAR α , PPAR γ , and adipocyte differentiation in vitro. *J. Nutr.* **2006**, *136*, 899–905. [[CrossRef](#)] [[PubMed](#)]
16. Kroker, A.J.; Bruning, J.B. Review of the Structural and Dynamic Mechanisms of PPAR γ Partial Agonism. *PPAR Res.* **2015**, *2015*, 1–15. [[CrossRef](#)] [[PubMed](#)]
17. Tolleson, W.H.; Doerge, D.R.; Churchwell, M.I.; Marques, M.M.; Roberts, D.W. Metabolism of biochanin A and formononetin by human liver microsomes in vitro. *J. Agric. Food Chem.* **2002**, *50*, 4783–4790. [[CrossRef](#)]
18. Groom, C.R.; Bruno, I.J.; Lightfoot, M.P.; Ward, S.C. The Cambridge Structural Database. *Acta Crystallogr. B* **2016**, *72*, 171–179. [[CrossRef](#)]
19. Caruso, F.; Incerpi, S.; Pedersen, J.Z.; Belli, S.; Kaur, S.; Rossi, M. Aromatic Polyphenol π - π Interactions with Superoxide Radicals Contribute to Radical Scavenging and Can Make Polyphenols Mimic Superoxide Dismutase Activity. *Curr. Issues Mol. Biol.* **2022**, *44*, 5209–5220. [[CrossRef](#)] [[PubMed](#)]
20. Caruso, F.; Berinato, M.; Hernandez, M.; Belli, S.; Smart, C.; Rossi, M. Antioxidant properties of bee propolis and an important component, galangin, described by X-ray crystal structure, DFT-D and hydrodynamic voltammetry. *PLoS ONE* **2022**, *17*, e0267624. [[CrossRef](#)] [[PubMed](#)]
21. Sheng, Y.; Abreu, I.A.; Cabelli, D.E.; Maroney, M.J.; Miller, A.F.; Teixeira, M.; Valentine, J.S. Superoxide dismutases and superoxide reductases. *Chem. Rev.* **2014**, *114*, 3854–3918. [[CrossRef](#)] [[PubMed](#)]
22. Fridovich, I. Superoxide radical and superoxide dismutases. *Annu. Rev. Biochem.* **1995**, *64*, 97–112. [[CrossRef](#)]
23. Belli, S.; Rossi, M.; Molasky, N.; Middleton, L.; Caldwell, C.; Bartow-McKenney, C.; Duong, M.; Chiu, J.; Gibbs, E.; Caldwell, A.; et al. Effective and novel application of hydrodynamic voltammetry to the study of superoxide radical scavenging by natural phenolic antioxidants. *Antioxidants* **2019**, *8*, 14. [[CrossRef](#)]
24. Caruso, F.; Rossi, M.; Kaur, S.; Garcia-Villar, E.; Molasky, N.; Belli, S.; Sitek, J.D.; Gionfra, F.; Pedersen, J.Z.; Incerpi, S. Antioxidant Properties of Embelin in Cell Culture. Electrochemistry and Theoretical Mechanism of Scavenging. Potential Scavenging of Superoxide Radical through the Cell Membrane. *Antioxidants* **2020**, *9*, 382. [[CrossRef](#)]
25. Okoye, I.; Yu, S.; Caruso, F.; Rossi, M. X-ray Structure Determination, Antioxidant Voltammetry Studies of Butein and 2',4'-Dihydroxy-3,4-dimethoxychalcone. Computational Studies of 4 Structurally Related 2',4'-diOH Chalcones to Examine Their Antimalarial Activity by Binding to Falcipain-2. *Molecules* **2021**, *26*, 6511. [[CrossRef](#)]
26. Ye, N.; Belli, S.; Caruso, F.; Roy, G.; Rossi, M. Antioxidant studies by hydrodynamic voltammetry and DFT, quantitative analyses by HPLC-DAD of clovamide, a natural phenolic compound found in *Theobroma Cacao* L. beans. *Food Chem.* **2021**, *341 Pt 2*, 128260. [[CrossRef](#)]
27. Shang, J.; Kojetin, D.J. Crystal Structure of Human PPAR γ Ligand Binding Domain in Complex with Edaglitazone. 2018. Available online: <https://www.rcsb.org/structure/5UGM> (accessed on 1 January 2022).
28. Sheldrick, G.M. Crystal structure refinement with SHELXL. *Acta Cryst.* **2015**, *C71*, 3–8. [[CrossRef](#)]
29. Macrae, C.F.; Sovago, I.; Cottrell, S.J.; Galek, P.T.A.; McCabe, P.; Pidcock, E.; Platings, M.; Shields, G.P.; Stevens, J.S.; Towler, M.; et al. Mercury 4.0: From visualization to analysis, design and prediction. *J. Appl. Crystallogr.* **2020**, *53 Pt 1*, 226–235. [[CrossRef](#)]
30. Mayrhofer, K.; Strmcnik, D.; Blizanac, B.; Stamenkovic, V.; Arenz, M.; Markovic, N. Measurement of oxygen reduction activities via the rotating disc electrode method: From Pt model surfaces to carbon-supported high surface area catalysts. *Electrochim. Acta* **2008**, *53*, 3181–3188. [[CrossRef](#)]
31. Delley, B.J. From molecules to solids with the DMol3 approach. *J. Chem. Phys.* **2000**, *113*, 7756–7764. [[CrossRef](#)]

32. Perdew, J.P.; Chevary, J.A.; Vosko, S.H.; Jackson, K.A.; Pederson, M.R.; Singh, D.J.; Fiolhais, C. Atoms, molecules, solids, and surfaces: Applications of the generalized gradient approximation for exchange and correlation. *Phys. Rev. B Cond. Mat. Mater. Phys.* **1992**, *46*, 6671–6687. [[CrossRef](#)]
33. Becke, A.D. Density-functional exchange-energy approximation with correct asymptotic behavior. *Phys. Rev. A* **1988**, *38*, 3098–3100. [[CrossRef](#)]
34. Grimme, S. Semiempirical GGA-type density functional constructed with a long-range dispersion correction. *J. Comput. Chem.* **2006**, *27*, 1787–1799. [[CrossRef](#)]
35. Wu, G.; Robertson, D.H.; Brooks, C.L.; Vieth, M.J. Detailed analysis of grid-based molecular docking: A case study of CDOCKER—A CHARMM-based MD docking algorithm. *J. Comput. Chem.* **2003**, *24*, 1549. [[CrossRef](#)] [[PubMed](#)]

Disclaimer/Publisher’s Note: The statements, opinions and data contained in all publications are solely those of the individual author(s) and contributor(s) and not of MDPI and/or the editor(s). MDPI and/or the editor(s) disclaim responsibility for any injury to people or property resulting from any ideas, methods, instructions or products referred to in the content.